Penerbit Akademia Baru

Journal of Advanced Research in Fluid Mechanics and Thermal Sciences

Journal homepage: www.akademiabaru.com/arfmts.html
ISSN: 2289-7879

Influence of Variable Liquid Properties on Mixed Convective MHD Flow over a Slippery Slender Elastic Sheet with Convective Boundary Condition

Open Access

K. V. Prasad[1] , Hanumesh Vaidya[2,*], K. Vajravelu[3], U. B. Vishwanatha[1]

[1] Department of Mathematics, VSK University, Vinayaka Nagar, Ballari-583 105, Karnataka, India
[2] Department of Mathematics, SSA Government First Grade College (Autonomous), Ballari-583 101, Karnataka, India
[3] Department of Mathematics, University of Central Florida, Orlando, FL 32816, USA

ARTICLE INFO

Article history:
Received 19 October 2018
Received in revised form 12 December 2018
Accepted 2 March 2019
Available online 11 April 2019

ABSTRACT

Mixed convective flow and heat transfer of MHD fluid over a variable thickened elastic surface with temperature dependent fluid properties is examined. The formulation is based on variable viscosity and thermal conductivity. In addition, velocity slip and convective boundary conditions are also taken into account. Obtained governing equations are cracked analytically using Optimal Homotopy Analysis method. Outcomes have been documented through graphs and tables, attained upshots are matched with previous existing results and are found to be in good agreement. Error tables and graphs have been plotted to prove the reliability and efficiency of the technique OHAM. A significant effect of Convective boundary conditions on flow and heat transfer has been noticed. For larger values of Biot number in the range $0.5 \leq \gamma \leq 5000$ the temperature of the fluid enhances.

Keywords:
Variable viscosity, thermal conductivity, wall thickness parameter, biot number

1. Introduction

A few engineering and modern applications include transport forms which are typically administered by mixed convection flows, for instance, heat exchangers, atomic reactors and electronic equipment and these procedures come to pass just when the impacts of buoyancy forces in forced convection become critical. On account of the flow over a horizontal heated or cooled surface, buoyancy impacts are not prominent and thus might be overlooked; in any case, for a vertical surface, the buoyancy compel produces critical consequences for the fluid flow and heat transfer through it. Contingent upon the forced flow bearing, the buoyancy forces may help or contradict (assisting mixed convection or restricting mixed convection) the forced flow, causing an expansion or reduction in heat transfer rate. In view of this, Schneider [1] examined the impact of buoyancy forces by considering first-order boundary layer theory and the obtained solutions cover the limited range

*Corresponding author.
E-mail address: hanumeshvaidya@gmail.com (Hanumesh Vaidya)

of buoyancy to forced convection parameter which does not include significant buoyant flows. Dey [2] extended the work of Schneider [1] to mass transfer. It is essential to note that both Ref. [1] and [2] did not explore the nature of the solution in the neighbourhood of separation. Afzal and Hussain [3] analyzed the solution beginning from purely free convection dominated to separate flows and obtained the dual solutions to the problem of Ref. [1]. Ingham [4] considered the presence of the double arrangements of the boundary layer equations of a consistently moving vertical plate with temperature conversely corresponding to the separation up the plate. Further, Wang [5] proposed that a mixed-convection parameter may replace the conventional Richardson number and introduced novel mixed-convection parameter to scale the commitment of the constrained and free convection appropriately. Ali and Al-Yousef [6] examined the work of Ingham [4] by considering suction or injection. Chen [7-8] registered the influence of the mixed convection on the vertical stretching sheet. Of late examinations that attention on the idea of mixed convection flow and heat transfer are seen in the literature [9-19]. The convective boundary condition at the boundary wall is another essential instrument in the investigation of boundary layer flow of fluid and is imperative in forms, for example, in a gas turbine, atomic plants, and warm vitality stockpiling. The pioneering work of Aziz [20] has encouraged several researchers to introduce convective boundary condition in their work. Aziz [20-21] examined the influence of convective boundary condition on a boundary layer flow of the classical Blasius problem over a flat surface. Makinde and Aziz [22] concluded that the thermal boundary is an increasing function of Biot number. Several researchers continued the work of Ref. [21] with different geometry (Bataller [23], Ishak *et al.,* [24], Yao *et al.,* [25] and Grosan *et al.,* [26])

Flow through the stretchable surface with variable thickness has many industrial applications such as architectural, mechanical, civil, aeronautical and marine engineering. It additionally helps to rot the heaviness of basic components and refine the usage of material. In any case, it is seen that little thought has been paid for the course through variable thickened surfaces. Fluid flow over a variable thickened surface is investigated by Fang *et al.,* [27]. By applying numerical FDM method Khader and Megahed [28] analyzed the flow of a Newtonian fluid through variable thickened nonlinear sheet by considering velocity slip. Hayat *et al.,* [29] examined via homotopy technique, the UCM fluid flow with Cattaneo-Christov heat flux model over a variable thickened surface. Recently, Prasad *et al.,* [30-33] employed OHAM/Keller box method and described the flow pattern over the variable thickened sheet.

The main objective of the present analysis is to forecast the behaviour of flow and heat transfer of MHD mixed convective liquid towards a variable thickened elastic sheet. Slip and convective boundary conditions are retained. Besides, the temperature dependent liquid properties, to mention, variable viscosity and variable thermal conductivity are also taken into account. The subsequent system of equations is solved for series solutions by implementing optimal homotopy algorithm (OHAM) [34-35]. Convergence analysis and error analysis of obtained solutions are confirmed overtly. Various thermophysical parameters on velocity and temperature fields are evaluated and plotted graphically. Skin friction and heat transfer rate are deliberated through different flow variables. With certain limiting conditions the present investigation is compared with published literature

2. Mathematical Formulation

Two-dimensional, steady incompressible mixed convective boundary layer flow of a viscous MHD fluid over a stretchable sheet is addressed. The thickness of the sheet is considered to be varying with the thickness $y = \mathrm{A}\left(x+b\right)^{(1-m)/2}$ where, A is a small constant and is chosen in such a way that the sheet is sufficiently thin so that pressure gradient can be avoided along the sheet $(\partial \mathrm{p}/\partial \mathrm{x} = 0)$.

The stretchable sheet is kept at a higher temperature T_w than the ambient temperature T_∞. A uniform magnetic field $B_0(x)$ is applied in the y direction normal to the sheet. The induced magnetic field is omitted because of the assumed small magnetic Reynolds number. The origin is located at the slot, from where the sheet is drawn in the fluid as depicted in Figure 1. Spontaneously two equal and opposite forces are applied along *x*-axis so as to stretch the sheet. The origin has been fixed at the center of the sheet with *x*-axis along the sheet and *y*-axis being normal to it. The flow is generated due to the stretching of the impermeable variable sheet which is restricted in domain y>0 with a velocity $U_w(x) = U_0(x + b)^m$ where U_0 is constant; *b* is a physical parameter related to stretching sheet and *m* is the velocity exponent parameter. Here, *m*>0 represents a decrease in the stretching sheet thickness due to the acceleration of the sheet whereas, *m*<0 increases thickness due to the deceleration of the sheet and *m*=1 represents flat sheet that is of uniform thickness.

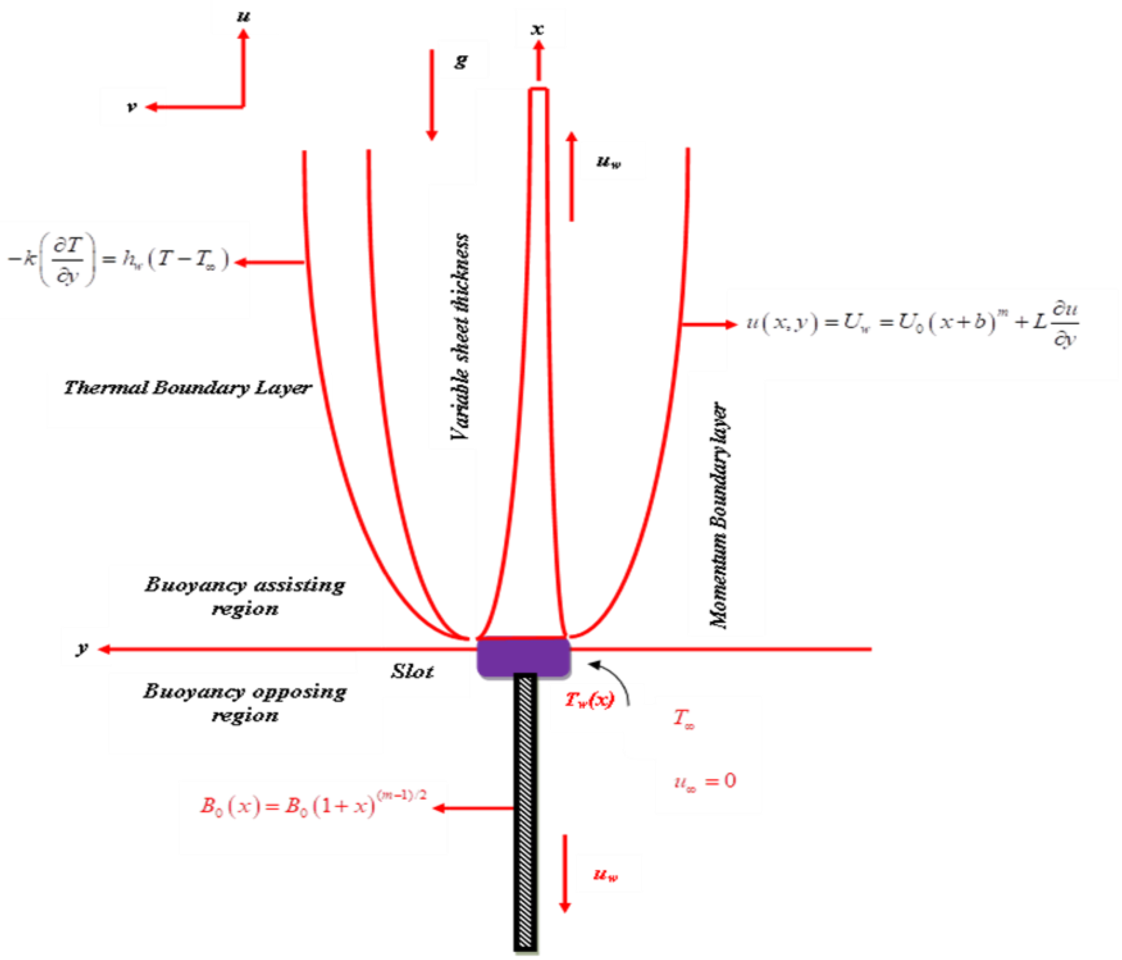

Fig. 1. Schematic diagram of the stretching sheet with variable thickness model

Figure 1 explains the physical description of the model. Under these assumptions and with Boussinesq approximations, the mass, momentum and energy equations in the presence of variable fluid properties are [32]

$$\frac{\partial u}{\partial x} + \frac{\partial v}{\partial y} = 0, \tag{1}$$

$$\rho_\infty\left(u\frac{\partial u}{\partial x}+\mathrm{v}\frac{\partial u}{\partial y}\right)=\frac{\partial}{\partial y}\left(\mu(T)\frac{\partial u}{\partial y}\right)\pm g\zeta\left(T-T_\infty\right)-\sigma\, B_0^2\left(x\right)u, \tag{2}$$

$$\rho_\infty c_p\left(u\frac{\partial T}{\partial x}+\mathrm{v}\frac{\partial T}{\partial y}\right)=\frac{\partial}{\partial y}\left(k\left(T\right)\frac{\partial T}{\partial y}\right) \tag{3}$$

where *u* and *v* are the fluid velocity components in the *x* and *y* directions respectively. ρ_∞ is the constant fluid density, g is the acceleration due to gravity, ζ is the coefficient of thermal expansion, "+" and "-" sign in the buoyancy term of Eq. (2) refers to buoyancy assisting and buoyancy opposing flow, respectively. C_p is the specific heat at constant pressure, σ is the electrical conductivity. A special form of the magnetic field is considered by many researchers [31] while studying magnetohydrodynamics which is defined as $B_0\left(x\right)=B_0\left(x+b\right)^{(m-1)/2}$. $\mu(T)$ and $k(T)$ are the temperature dependent viscosity and thermal conductivity [33] and are given by

$$\mu(T)=\frac{\mu_\infty}{\left[1+\delta\left(T-T_\infty\right)\right]}\ \text{and}\ k(T)=k_\infty\left(1+\frac{\varepsilon}{\Delta T}\left(T-T_\infty\right)\right) \tag{4}$$

where T_∞, μ_∞ and k_∞ are the constant temperature, viscosity and thermal conductivity of the fluid far away from the sheet respectively, δ is a small parameter reflecting a thermal property of a fluid, ε is variable thermal conductivity parameter, $\Delta T=T_w-T_\infty=\left(C/l\right)\left(x+b\right)^r$, where T_w is the sheet temperature, *C* is a constant, *l* is the characteristic length, ε is the thermal conductivity parameter and k_∞ is thermal conductivity of the fluid away from the sheet, *r* is a wall temperature parameter. Variable fluid viscosity $\mu(T)$ can also be written as $\mu^{-1}=a\left(T-T_r\right)$ where, $a=\delta/\mu_\infty$ and $T_r=T_\infty-\left(1/\delta\right)$. a and T_r are constants whose values depend on both the reference state and the thermal properties of the fluid. Usually, $a>0$ corresponds to a liquid and $a<0$ for gasses. Buoyancy force assists the flow in the upper half of the region and in the lower half it opposes the flow as shown in the Figure 1. $x-$axis points upwards in the direction of the stretching hot surface for the assisting flow whereas for the opposing flow $x-$axis points vertically downwards in the direction of the stretching hot surface. Exactly the reverse phenomenon occurs if the sheet is cooled below the ambient temperature.

Boundary conditions for the problem are

$$u\left(x,y\right)=U_w=U_0\left(x+b\right)^m+L\left(x\right)\frac{\partial u}{\partial y},\mathrm{v}\left(x,y\right)=0,\ -k\left(\frac{\partial T}{\partial y}\right)=h_w\left(x\right)\left(T-T_\infty\right)\ at\ \ y=A\left(x+b\right)^{\frac{1-m}{2}},$$
$$u\left(x,y\right)\to 0,\qquad T\left(x,y\right)\to T_\infty\ \ as\ \ y\to\infty. \tag{5}$$

It should be noted that a positive m indicates stretching and a negative value indicates a shrinking sheet, $L\left(x\right)=L\left(x+b\right)^{\frac{1-m}{2}}$ is the local molecular mean free path (is always positive) and, $h_w\left(x\right)=h_w\left(x+b\right)^{\frac{1-m}{2}}$ is the local heat transfer coefficient.

3. Similarity Transformations

Let the dimensionless similarity variable be

$$\eta = y\sqrt{\frac{m+1}{2}\frac{U_0}{\nu_\infty}}\,(x+b)^{\frac{m-1}{2}} \tag{6}$$

the stream function $\psi(x,y)$ and the dimensionless temperature distribution $\theta(\eta)$ be

$$\psi(x,y) = f(\eta)\sqrt{\frac{2}{m+1}U_0\nu_\infty}\,(x+b)^{\frac{m+1}{2}},\ \theta(\eta)=\frac{(T-T_\infty)}{(T_w-T_\infty)} \tag{7}$$

Using (7) the velocity components can be written as [35]

$$(u,v)=\left(U_w\frac{df(\eta)}{d\eta},-\sqrt{\nu_\infty\frac{m+1}{2}U_0}\,(x+b)^{\frac{m-1}{2}}\left[f(\eta)+\eta\frac{df(\eta)}{d\eta}\left(\frac{m-1}{m+1}\right)\right]\right) \tag{8}$$

It is presumed that $m>-1$ for the validity of the similarity variable. Using Eq. (4),(6) - (8) Eq. (2), (3) and (5) reduces to

$$\frac{d}{d\eta}\left(\frac{d^2f}{d\eta^2}(1-\theta/\theta_r)^{-1}\right)+f\frac{d^2f}{d\eta^2}-\frac{2m}{(m+1)}\left(\frac{df}{d\eta}\right)^2-Mn\frac{df}{d\eta}+\lambda\theta=0, \tag{9}$$

$$\frac{d}{d\eta}\left[(1+\varepsilon\theta)\frac{d\theta}{d\eta}\right]+\Pr\left(f\frac{d\theta}{d\eta}-\frac{2r}{m+1}\theta\frac{df}{d\eta}\right)=0, \tag{10}$$

The fluid viscosity parameter θ_r, magnetic parameter Mn, buoyancy parameter λ and Prandtl number Pr are non dimensional which defined as

$$\theta_r=\frac{T_r-T_\infty}{T_w-T_\infty},\quad Mn=\frac{2\sigma B_0^2}{\rho_\infty U_0(1+m)},\quad \lambda=\frac{\pm 2g\zeta C}{l(1+m)U_0^2}\ \text{and}\ \Pr=\frac{\nu_\infty}{\alpha_\infty}.$$

The mixed convection parameter λ is independent of x only if $r=2m-1$. On another hand, $\lambda=O(1)$ for combined convective flow, if λ is of a greater order of magnitude than unity, the buoyancy forces will be dominant and the flow will essentially be free convective. Further, as θ_r is inversely proportional to the temperature difference $(T_\infty-T_w)$, the effect of variable viscosity is neglected for larger values of θ_r. On another hand, variable viscosity becomes significant for smaller values of θ_r due to the fact that the fluid viscosity changes (decreases with increase in temperature) noticeably with temperature. It is important to note that for liquids θ_r < 0 and for gases θ_r > 0.
The corresponding boundary conditions are $(m\neq 1)$

$$f(\alpha)=\alpha\frac{1-m}{1+m},\ f'(\alpha)=1+\beta f''(\alpha)\ \text{and}\ \theta'(\alpha)=-\gamma\left(1-\theta(\alpha)\right)\ \text{at}\ \alpha=0$$
$$f'(\alpha)=\theta(\alpha)=0\ \text{at}\ \alpha\to\infty. \tag{11}$$

where,

$$\alpha=A\sqrt{\frac{m+1}{2}\frac{U_0}{\nu_\infty}},\beta=\frac{L\alpha}{A},\gamma=\frac{h_w A}{\alpha k_\infty}$$

are respectively the wall thickness parameter, velocity slip parameter and Biot number. Here

$$\eta=\alpha=A\sqrt{\frac{m+1}{2}\frac{U_0}{\nu_\infty}}$$

indicates the plate surface. The following variable transformation has been used in order to assist simulations and the solution domain is fixed from 0 to ∞. $f(\xi)=f(\eta-\alpha)=f(\eta)$ and $\theta(\xi)=\theta(\eta-\alpha)=\theta(\eta)$. Now the Eq. (9), (10) and (11) reduces to

$$\left(f''(1-\theta/\theta_r)^{-1}\right)'+ff''-\frac{2m}{(m+1)}f'^2-Mn\,f'+\lambda\theta=0, \tag{12}$$

$$\left[(1+\varepsilon\theta)\theta'\right]'+\Pr\left(f\theta'-\frac{2(2m-1)}{m+1}\theta f'\right)=0. \tag{13}$$

corresponding boundary conditions are $(m\neq1)$

$$f(\xi)=\alpha\frac{1-m}{1+m},\ f'(\xi)=1+\beta f''(0)\ ,\theta'(\xi)=-\gamma\left(1-\theta(\xi)\right)\ \text{at}\ \xi=0$$
$$f'(\xi)=\theta(\xi)=0\ \text{at}\ \xi\to\infty \tag{14}$$

where the prime denotes the differentiation with respect to ξ. $f''(\xi)=f''(0)$ and $\theta'(\xi)=\theta'(0)$ are now the shear stress and wall temperature gradient respectively.

The important physical parameters are local skin friction C_{fx} and the local Nusselt number Nu_x which are defined as:

$$C_{fx}=\frac{\tau_w}{\rho_\infty U_w^2/2}\ \text{and}\ Nu_x=\frac{xq_w}{k_\infty(T_w-T_\infty)}$$

where,

$$\tau_w=\mu(T)\left.\frac{\partial u}{\partial y}\right|_{y=A(x+b)^{\frac{1-m}{2}}}\ \text{and}\ q_w=-k(T)\left.\frac{\partial T}{\partial y}\right|_{y=A(x+b)^{\frac{1-m}{2}}}$$

Using similarity transformations, we get

$$C_{f_x} = \frac{2\nu_\infty \left(u_y\right)_{y=A(x+b)^{\frac{1-m}{2}}}}{U_w^2} = 2\sqrt{(m+1)/2}\,\left(\mathrm{Re}_x\right)^{-1/2} f''(0),$$
$$Nu_x = \frac{(x+b)\left(T_y\right)_{y=A(x+b)^{\frac{1-m}{2}}}}{\left(T_w - T_\infty\right)} = -\sqrt{(m+1)/2}\,\left(\mathrm{Re}_x\right)^{1/2}\theta'(0), \tag{15}$$

where, $\mathrm{Re}_x = \dfrac{U_w(x+b)}{\nu_\infty}$ is the local Reynolds number.

4. Semi-analytical Solution: Optimal Homotopy Analysis Method (OHAM)

Optimal homotopy analysis method has been employed to solve the coupled non-linear system of Eq. (12) and (13) with boundary conditions (14). In accordance with the boundary conditions, consider the base functions as $\{e^{(-n\xi)} / n \geq 0\}$ then, the dimensionless velocity $f(\xi)$ and temperature $\theta(\xi)$ can be expressed in the series form as follows

$$f(\xi) = \sum_{n=0}^{\infty} a_n\, e^{(-n\xi)} \text{ and } \theta(\xi) = \sum_{n=0}^{\infty} b_n\, e^{(-n\xi)}$$

where a_n and b_n are the coefficients. According to the rule of solution expression and boundary conditions, we assume the following studies reported by Liao [34] and Van Gorder [35]. Let initial guesses and the linear operators for $f(\xi)$ and $\theta(\xi)$ be

$$f_0(\xi) = \left(\frac{1}{1+\beta}\right)\left(1-e^{-\xi}\right) + \alpha\frac{1-m}{1+m} \text{ and } \theta_0(\xi) = \left(\frac{\gamma}{1+\gamma}\right)e^{-\xi},\ L_f = \frac{d^3}{d\xi^3} - \frac{d}{d\xi} \text{ and } L_\theta = \frac{d^2}{d\xi^2}. \tag{16}$$

such that $L_f[c_1 + c_2 e^{\xi} + c_3 e^{-\xi}] = 0$ and $L_\theta[c_4 e^{\xi} + c_5 e^{-\xi}] = 0$ where c_i's $(i = 1,2,3,4,5)$ are arbitrary constants. Auxiliary function as $H_f(\eta) = H_\theta(\eta) = e^{-\xi}$. Let us consider so called zeroth order deformation equation

$$(1-q)L_f\left[\hat{f}(\xi,q) - f_0(\xi)\right] = qH_f(\xi)\hbar_f N_f\left[\hat{f}(\xi,q), \hat{\theta}(\xi,q)\right], \tag{17}$$

$$(1-q)L_\theta\left[\hat{\theta}(\xi,q) - \theta_0(\xi)\right] = qH_\theta(\eta)\hbar_\theta N_\theta\left[\hat{\theta}(\xi,q), \hat{f}(\xi,q)\right], \tag{18}$$

with conditions

$$\hat{f}(0,q) = \alpha\frac{1-m}{1+m},\ \hat{f}'(0,q) = 1 + \beta\hat{f}''(0,q),\ \hat{f}(\infty,q) = 0;$$
$$\hat{\theta}'(0,q) = -\gamma\left(1 - \hat{\theta}(0,\eta)\right),\ \hat{\theta}(\infty,q) = 0. \tag{19}$$

where, $q \in [0,1]$ is an embedding parameter, $\left(\hbar_f, \hbar_\theta\right) \neq 0$ are the convergence control parameters and N_f and N_θ are non-linear operators defined as

$$N_f = \left(1 - \frac{\hat{\theta}(\xi,q)}{\theta_r}\right)\hat{f}'''(\xi,q) + \frac{\hat{f}''(\xi,q)\hat{\theta}'(\xi,q)}{\theta_r} + \left(1 - \frac{\hat{\theta}(\xi,q)}{\theta_r}\right)^2 \hat{f}(\xi,q)\,\hat{f}''(\xi,q)$$
$$-\left(1 - \frac{\hat{\theta}(\xi,q)}{\theta_r}\right)^2 \frac{2m}{m+1}\hat{f}(\xi,q)^2 - \left(1 - \frac{\hat{\theta}(\xi,q)}{\theta_r}\right)^2 Mn\,\hat{f}'(\xi,q) + \lambda\left(1 - \frac{\hat{\theta}(\xi,q)}{\theta_r}\right)^2 \hat{\theta}(\xi,q),$$
$$N_\theta = \left(\left(1 + \varepsilon\,\hat{\theta}(\xi,q)\right)\hat{\theta}'(\xi,q)\right)' + \Pr\left(\hat{f}(\xi,q)\hat{\theta}'(\xi,q) - \frac{2(2m-1)}{m+1}\hat{\theta}(\xi,q)\,\hat{f}'(\xi,q)\right)$$

From Eq. (17) - (18), at $q=0$ we have $L_f\left[\hat{f}(\xi,0) - f_0(\xi)\right] = 0$ and $L_\theta\left[\hat{\theta}(\xi,0) - \theta_0(\xi)\right] = 0$ which implies that $\hat{f}(\xi,0) = f_0(\xi)$ and $\hat{\theta}(\xi,0) = \theta_0(\xi)$ respectively, whereas, at $q=1$ we have $N_f\left[\hat{f}(\xi,1), \hat{\theta}(\xi,1)\right] = 0$ and $N_\theta\left[\hat{\theta}(\xi,1), \hat{f}(\xi,1)\right] = 0$ which implies that $\hat{f}(\xi,1) = f(\xi)$ and $\hat{\theta}(\xi,1) = \theta(\xi)$ respectively. Hence, by defining

$$f_m(\xi) = \frac{1}{m!}\frac{d^m f(\xi,q)}{d\xi^m}\bigg|_{q=0}, \theta_m(\xi) = \frac{1}{m!}\frac{d^m \theta(\xi,q)}{d\xi^m}\bigg|_{q=0}$$

we expand $\hat{f}(\xi,q)$ and $\hat{\theta}(\xi,q)$ by means of Taylor's series as

$$\hat{f}(\xi,q) = f_0(\xi) + \sum_{m=1}^{\infty} f_m(\xi)q^m \text{ and } \hat{\theta}(\xi,q) = \theta_0(\xi) + \sum_{m=1}^{\infty}\theta_m(\xi)q^m. \tag{20}$$

If the series (20) converges at q = 1, we get the homotopy series solution as

$$f(\xi) = f_0(\xi) + \sum_{m=1}^{\infty} f_m(\xi) \text{ and } \theta(\xi) = \theta_0(\xi) + \sum_{m=1}^{\infty}\theta_m(\xi) \tag{21}$$

4.1 Optimal Convergence-Control Parameter

It should be noted that $f(\xi)$ and $\theta(\xi)$ in Eq. (21) contain unknown convergence control parameters $\hbar_f$ and $\hbar_\theta$, which can be used to adjust and control the convergence region and the rate of convergence of the homotopy series solution. m^{th} order deformation equations and the conditions are

$$L_f\left[f_m(\xi) - \chi_m f_{m-1}(\xi)\right] = H_f(\xi)\hbar_f\, R_m^{\,f}(\xi),$$
$$L_\theta\left[\theta_m(\xi) - \chi_m \theta_{m-1}(\xi)\right] = H_\theta(\xi)\hbar_\theta\, R_m^{\,\theta}(\xi),$$

With $f_m(0)=0,\ f_m{}'(0)=1+\beta f_m''(0),\ f_m{}'(\infty)=0,$
$\theta_m'(0)=-\gamma\left(1-\theta_m(0)\right),\ \theta_m(\infty)=0$

$$R_m{}^f = f_{m-1}'''(\eta)-\left(\frac{1}{\theta_r}\right)\sum_{k=0}^{m-1} f_{m-1-k}'''\theta_k+\left(\frac{1}{\theta_r}\right)\sum_{k=0}^{m-1} f_{m-1-k}''\theta_k'+\sum_{k=0}^{m-1} f_{m-1-k}'' f_k$$
$$+\frac{1}{\theta_r{}^2}\sum_{k=0}^{m-1} f_{m-1-k}''\sum_{j=0}^{k} f_{k-j}\sum_{i=0}^{j}\theta_{j-i}\theta_i-\frac{2}{\theta_r}\sum_{k=0}^{m-1} f_{m-1-k}''\sum_{j=0}^{k} f_{k-j}\theta_j$$
$$-\left(\frac{2m}{m+1}\right)\sum_{k=0}^{m-1} f_{m-1-k}' f_k'-\left(\frac{2m}{m+1}\right)\left(\frac{1}{\theta_r{}^2}\right)\sum_{k=0}^{m-1} f_{m-1-k}'\sum_{j=0}^{k} f_{k-j}'\sum_{i=0}^{j}\theta_{j-i}\theta_i$$
$$+\left(\frac{2m}{m+1}\right)\left(\frac{2}{\theta_r}\right)\sum_{k=0}^{m-1} f_{m-1-k}'\sum_{j=0}^{k} f_{k-j}'\theta_j-Mn\, f_{m-1}'(\xi)-Mn\left(\frac{1}{\theta_r{}^2}\right)\sum_{k=0}^{m-1} f_{m-1-k}'\sum_{j=0}^{k}\theta_{k-j}\theta_j$$
$$+2\,Mn\left(\frac{1}{\theta_r}\right)\sum_{k=0}^{m-1} f_{m-1-k}'\theta_k+\lambda\theta_{m-1}(\xi)+\lambda\left(\frac{1}{\theta_r{}^2}\right)\sum_{k=0}^{m-1}\theta_{m-1-k}\sum_{j=0}^{k}\theta_{k-j}\theta_j$$
$$-\lambda\left(\frac{2}{\theta_r}\right)\sum_{k=0}^{m-1}\theta_{m-1-k}\theta_k$$

where,

$$R_m{}^\theta=\theta_{m-1}''(\eta)+\varepsilon\left(\sum_{k=0}^{m-1}\theta_{m-1-k}''\theta_k+\sum_{k=0}^{m-1}\theta_{m-1-k}'\theta_k'\right)+\Pr\sum_{k=0}^{m-1}\theta_{m-1-k}' f_k-\left(\frac{2(2m-1)}{m+1}\right)\Pr\sum_{k=0}^{m-1} f_{m-1-k}'\theta_k$$

and $\chi_m=\begin{cases}0, m\le 1\\ 1, m>1\end{cases}.$

4.2 Error Analysis

The error is evaluated and minimized over $\hbar_f$ and $\hbar_\theta$ in order to obtain the optimal value of $\hbar_f$ and $\hbar_\theta$. At k^{th} order deformation equation, the exact residual error is given by

$$\hat{E}_k{}^f=\int_0^1\left(N_f\left[\sum_{n=0}^{k} f_n(\xi)\right]\right)^2 d\xi \text{ and } \hat{E}_k{}^\theta=\int_0^1\left(N_\theta\left[\sum_{n=0}^{k}\theta_n(\xi)\right]\right)^2 d\xi.$$

But in practice, the evaluation of $\hat{E}_k{}^f$ and $\hat{E}_k{}^\theta$ is much time consuming so instead of exact residual error we use average residual error defined as

$$E_k{}^f=\frac{1}{M+1}\sum_{l=0}^{M}\left(N_f\left[\sum_{n=0}^{k} f_n(\xi_l)\right]\right)^2 \text{ and } E_k{}^\theta=\frac{1}{M+1}\sum_{l=0}^{M}\left(N_\theta\left[\sum_{n=0}^{k}\theta_n(\xi_l)\right]\right)^2,\ E_k^t=E_k{}^f+E_k{}^\theta$$

where, $E_m{}^t$ is the total squared residual error, $\xi_l=l\Delta\xi=\frac{l}{M}, l=0,1,2,....M$. Now the error function $E_k{}^f$ and $E_k{}^\theta$ is minimized over $\hbar_f$ and $\hbar_\theta$ to obtain the optimal values. Table 1 lists the values of individual average residual errors by considering the optimal values of $h_f(-0.955139)$ and $h_\theta(-1.065420)$, which has been obtained by minimizing the squared residual errors of f and θ at the approximation $k=10$ as shown in Table 2. For f and θ CPU consumes more and more time as the order of approximation increases and noticeably the average residual error reduces monotonically which is recorded in Table 1. Hence the quick convergence of solution series is obtained with the assistance of optimal value of f and θ . Validation of the present method is executed by comparing the present results $\left(f''(0)\right)$ with the results of Fang *et al.,* [27], Khader and Megahed [28] and Prasad *et al.,* [33] which are found to be complete agreement (Table 3). This error is obtained by evaluating the absolute difference between the present skin friction [27,28,33], and thereafter, this difference is divided by the present skin friction and the resultant is multiplied by 100, to obtain the percentage of the relative error [36,37].

5. Results and Discussions

The pertinent parameters entering into the fluid are fluid viscosity parameter (θ_r), the mixed convection parameter (λ), the thermal conductivity parameter (ε), the velocity power index parameter (*m*) and the Prandtl number (Pr), the velocity slip parameter (β), the magnetic parameter (Mn), the wall thickness parameter (α) and Biot number (γ) and these are examined through plotting graphs (Figure 2-9) for the horizontal velocity profile $f'(\xi)$, the temperature field $\theta(\xi)$. The profiles of these graphs tend asymptotically to zero. The skin friction $\left(f''(0)\right)$ and wall temperature gradient $\left(\theta'(0)\right)$ are tabulated in Table 4.

The impact of θ_r and α on $f'(\xi)$ and $\theta(\xi)$ is elucidated in Figure 2 (a-b). It is explicit from Figure 2 (a) that $f'(\xi)$ decreases for larger values θ_r. This behaviour of velocity profile may be attributed to fact that the fluid viscosity depends inversely on the temperature difference between the wall and the ambient fluid, $\left(\theta_r = -\left(\delta\left(T_w - T_\infty\right)\right)^{-1}\right)$, so, reduction in momentum boundary layer thickness. On the other hand, the quiet opposite impact is observed on the temperature profile (see Figure 2(b)).

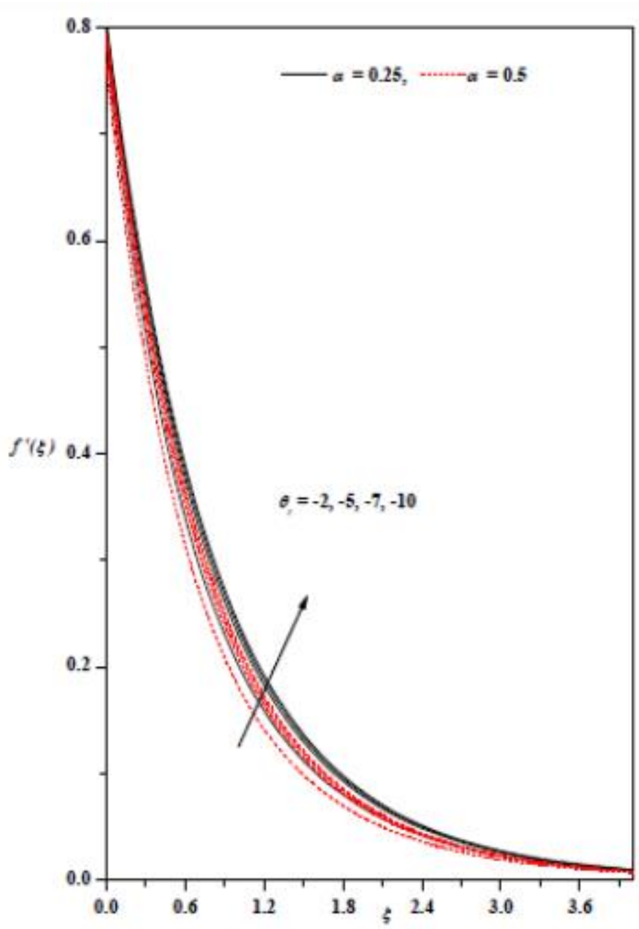

Fig. 2(a). Horizontal velocity profile for different values of θ_r and α with Mn = 1, γ = 5, λ= 0.2, β = 0.2, ε = 0.2, *m*= 0.25, $\Pr$ = 0.72

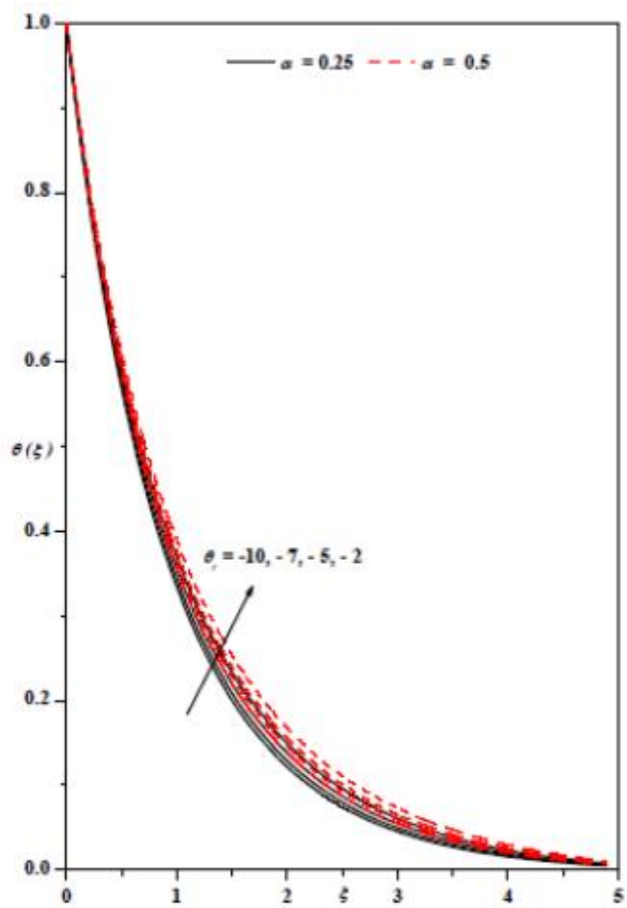

Fig. 2(b). Temperature profile for different values of θ_r and α with Mn = 1, γ = 5, λ= 0.2, β = 0.2, ε = 0.2, *m*= 0.25, $\Pr$ = 0.72

Figure 3 (a) and 3(b) represents the effect of λ on dimensionless velocity and temperature field. Due to the enhanced mixed convection parameter $(\lambda = \text{-}1, 0.\ 0.5, 1, 2)$ velocity profile increases and temperature profile decreases. Here, hotness (assisting flow) and coldness (opposing flow) of the fluid purely depends on positive and negative values of λ (that is λ>0 *and* λ<0).

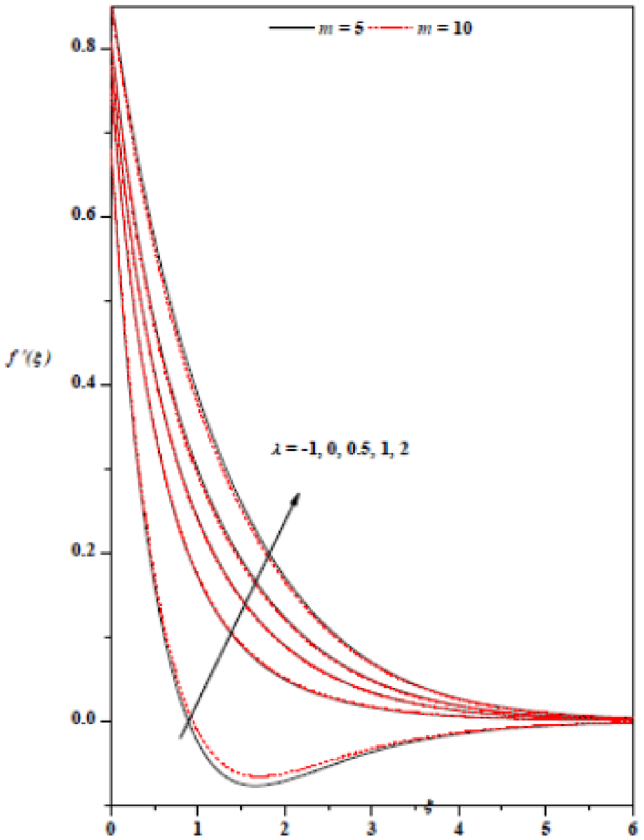

Fig. 3(a). Horizontal velocity profile for different values of λ and m with θ_r = -2, γ = 5, α = 0.25, β = 0.2, Pr = 0.72, ε = 0.2, Mn = 1

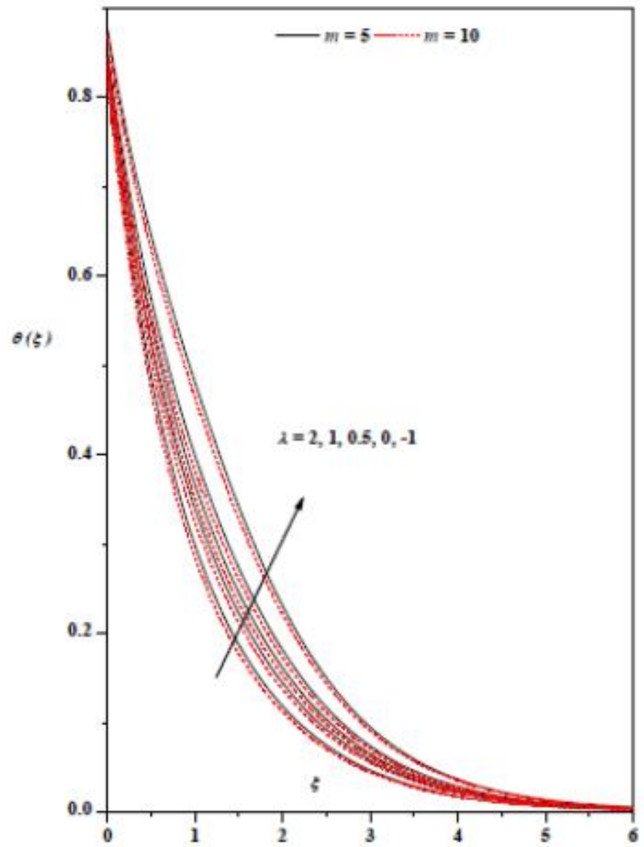

Fig. 3(b). Temperature profile for different values of λ and m with θ_r = -2, γ = 5, α = 0.25, β = 0.2, Pr = 0.72, ε = 0.2, Mn = 1

Figure 4 (a) illustrates the effect of Mn on $f'(\xi)$ and $\theta(\xi)$ for different values of α. The upsurge in the Magnetic parameter Mn results in diminished velocity profile, this is due to the reason that the fluid is considered to be electrically conducting which is responsible for the transverse magnetic field and Lorentz forces, resists the transport phenomena hence velocity profile and consequently, the momentum boundary layer thickness decreases. As the Lorentz force resists the transport phenomena, friction between the layers increases and hence the temperature profile increases (see Figure 4(b)).

Figure 5 (a)-5(b) exhibit the effect of *m* on $f'(\xi)$ and $\theta(\xi)$ for different values of α, it is noticed that for growing the value of *m* both velocity and temperature profile decreases consequently, the momentum and thermal boundary layer thickness decreases. It is important to note from all the above that the $f'(\xi)$ at any point near the surface decrease as the wall thickness parameter increase for $m < 1$ and becomes thinner for $\theta(\xi)$ when $m < 1$ and a reverse is true for $m \geq 1$.

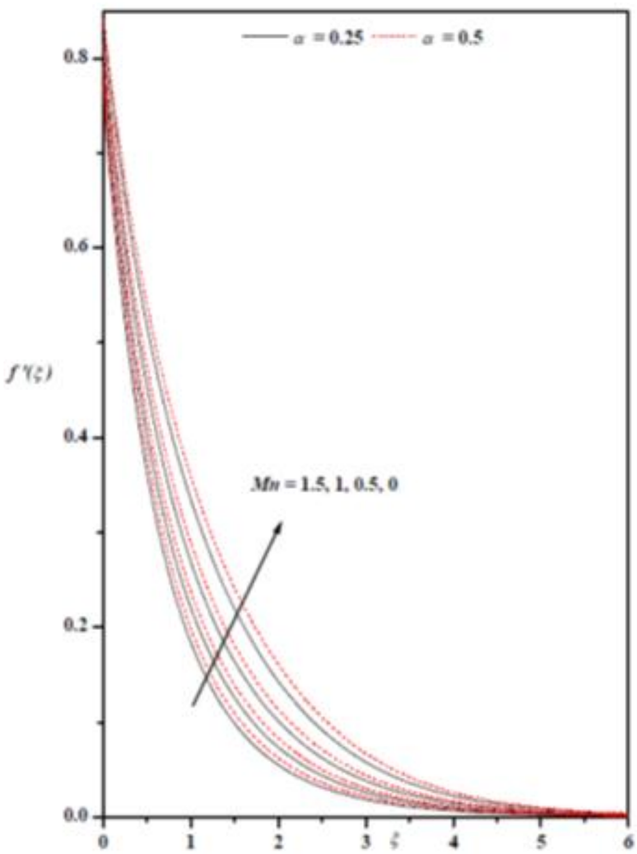

Fig. 4(a). Horizontal velocity profile for different values of Mn and α with θ_r = -5, γ =5, λ =0.2, $\Pr$ =0.2, ε =0.72, m =5, β =0.2

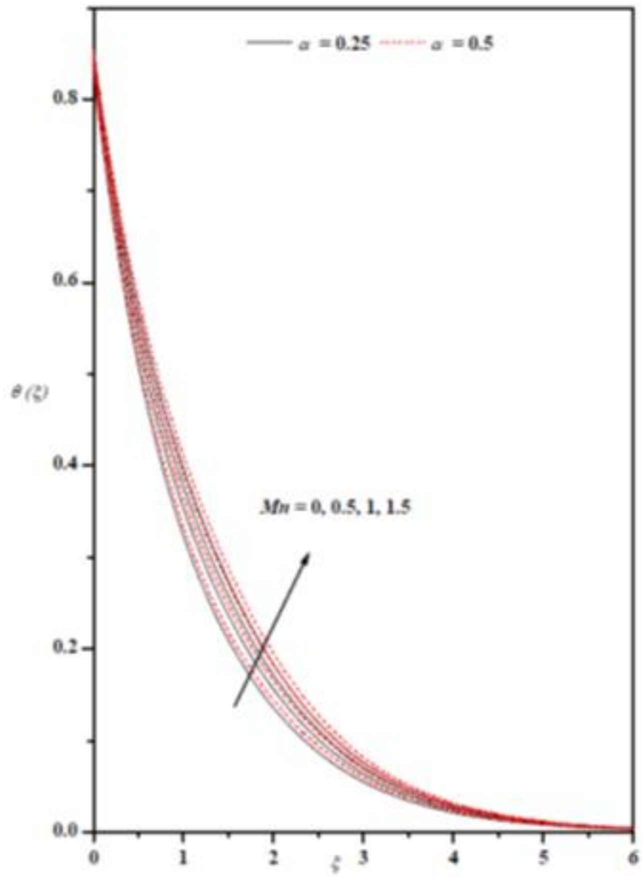

Fig. 4(b). Temperature profile for different value Mn and α with θ_r = -5, γ =5, λ =0.2, $\Pr$ =0.2, ε =0.72, m =5, β =0.2

The larger values of γ makes a substantial impact on fluid flow which is shown in Figure 6. As a result of higher values of Biot number $(\gamma = 0.5, 1, 5, 10, 50, 100, 500, 1000, 5000)$, temperature profile reaches peak and enhancement in the thickness of the thermal boundary layer is noticed. From the point of theoretical analysis, the Biot number is the proportion of inner conductive resistance from outside convective resistance which defines the relation between convection and conduction heat transfer phenomena. However, a smaller value of Biot number $(\gamma < 1)$ demonstrates that the conduction is the primary heat transfer strategy, while high estimations of this number $(\gamma > 1)$ show that the convection is the principal heat transfer instrument. Figure 7 depicts the effect of the slip parameter (β) on velocity $f'(\xi)$ for different values m. As the slip parameter increases the velocity profile also increases, showing that the skin friction increases at the surface (Table 4). Physically, this infers the frictional opposition between the surface and liquid molecule increments, therefore, the velocity of the liquid declines. Figure 8 sketched to show the impact on $\Pr = 6.2, 5.09, 2, 1, 0.72$ on $\theta(\xi)$, it shows that temperature profile decreases with an increase in Pr. From the trial considers it has been noticed that at 20^{0}C the Prandtl number for air is 0.72, at 300^0 C the Prandtl number for water is 1.09, at 40^0 C the Prandtl number for ammonia is 2.0 and at 417^0 C the Prandtl number for molten salt is 5.09 [33]. Prandtl number $(\Pr = \nu_\infty / \alpha_\infty)$ signifies the thickness of the thermal boundary layer which depends on whether $\Pr = 1, \Pr > 1$ or $\Pr < 1$. This analysis clears that the higher heat transfer rate can be achieved by considering the lower Prandtl number. The reverse trend can be observed with reference to ε (See Figure 9). Figure 10(a-b) presents the 3D flow design investigation. The reverse trend can be observed with reference to ε (See Figure 9). Figure 10(a-b) presents the 3D flow design of the thought about the investigation. The velocity of the fluid strongly relies upon the initial velocity of the wall can be noted. Furthermore, Figure 11(a-b) is plotted to discover the streamline patterns when for different values of velocity power index parameter *m*. It can be seen that application of *m* causes a disturbance in the flow and heat transfer pattern of the fluid.

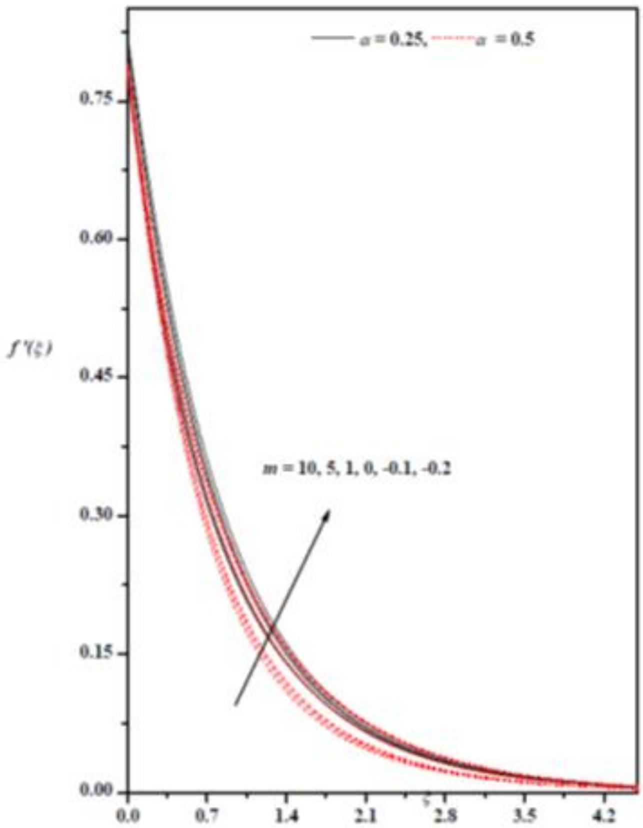

Fig. 5(a). Horizontal velocity profile for different values of m and α with θ_r = -5, γ =5, β =0.2, $\Pr$ = 0.72, ε = 0.2, Mn =1

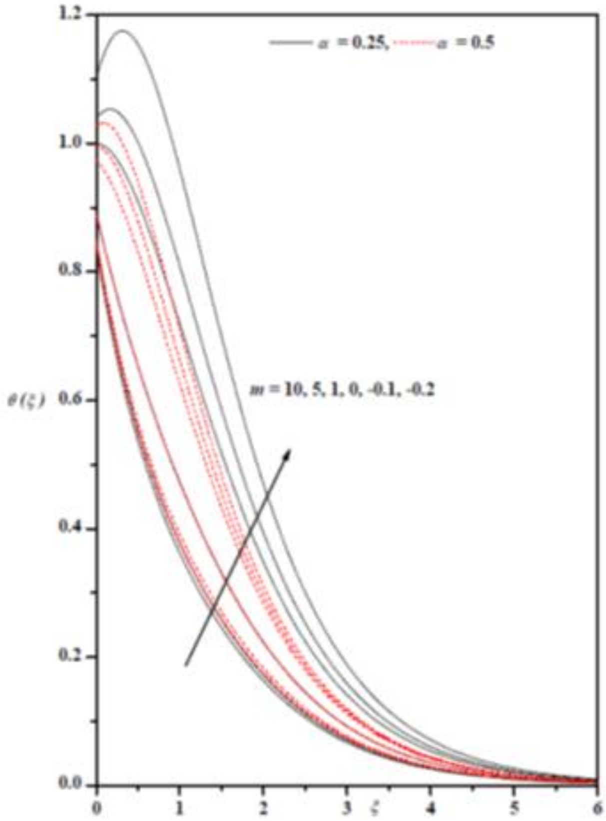

Fig. 5(b). Temperature profile for different values of m and α with θ_r = -5, γ =5, β = 0.2, $\Pr$ = 0.72, ε = 0.2, Mn =1

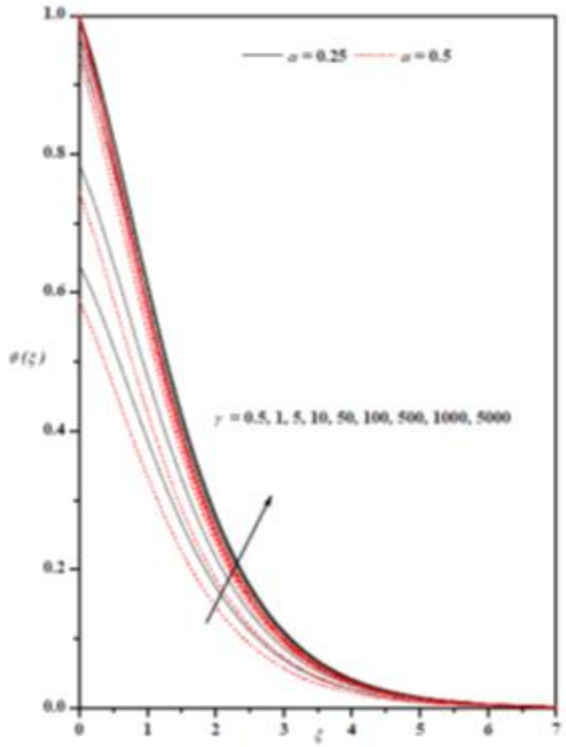

Fig. 6. Temperature profile for different value α and γ with θ_r = -5, m = 0.25, ε = 0.1, β = 0.1, Pr = 0.72, α = 0.5, Mn = 0.1

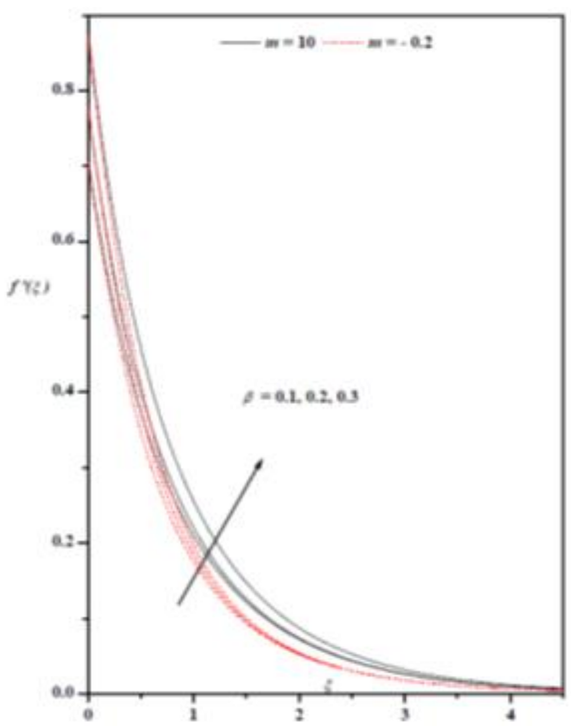

Fig. 7. Horizontal velocity profile for different values of β and m with θ_r = -5, Mn = 1, γ = 5, Pr = 0.72, m =10, ε = 0.2, α = 0.25, λ = 0.2

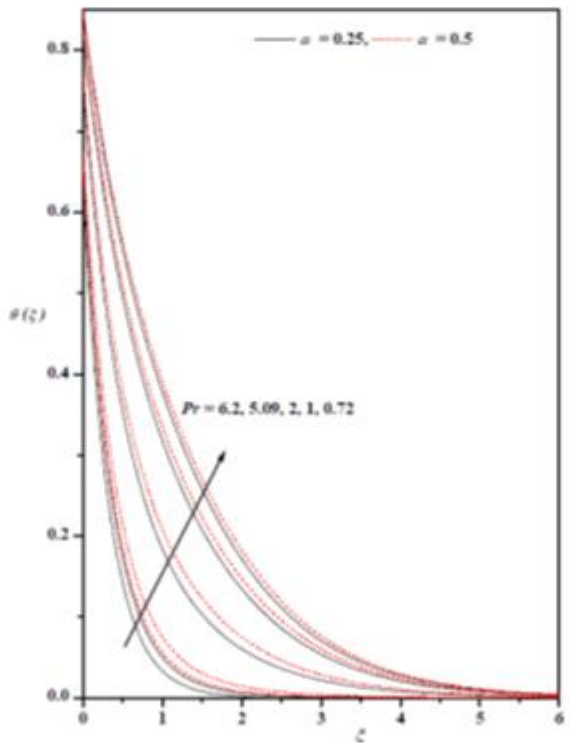

Fig. 8. Temperature profile for different value Pr and α with θ_r = -5, γ = 5, λ = 0.2, β = 0.2 ε = 0.2, m = 5, Mn = 1

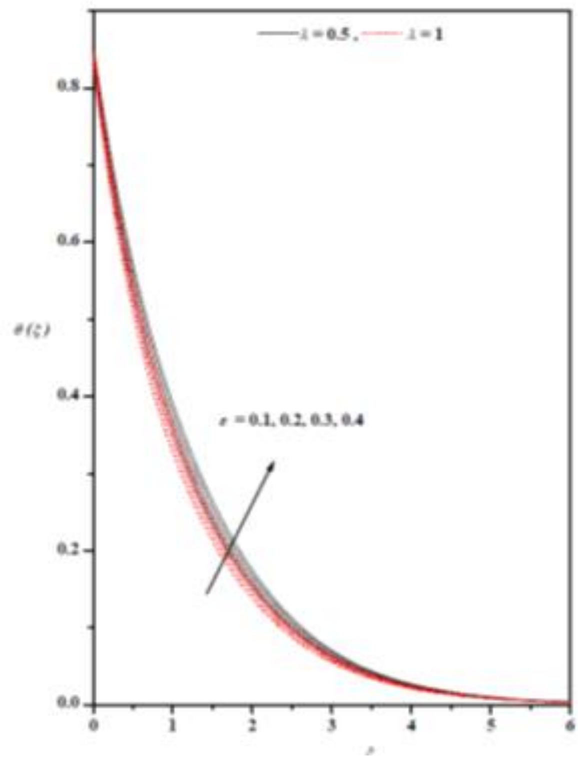

Fig. 9. Temperature profile for different value ε and λ with θ_r = -2, m = 5, γ = 5, β = 0.2, Pr =0.72, α = 0.25, Mn = 1

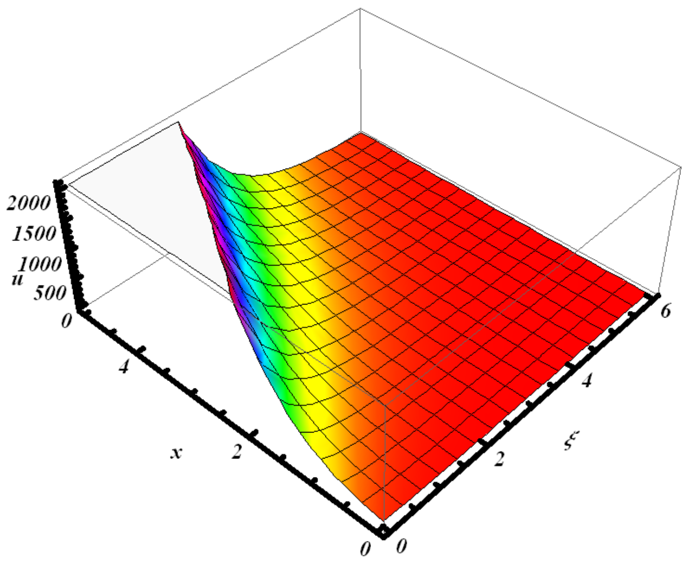

Fig. 10(a). 3D plot of u with ξ and x for
$Pr = 0.72, \varepsilon = 0.2, \theta_r = -5, \alpha = 0.5, m = 5, Mn = 1.5, \gamma = 5, \lambda = \beta = 0.2.$

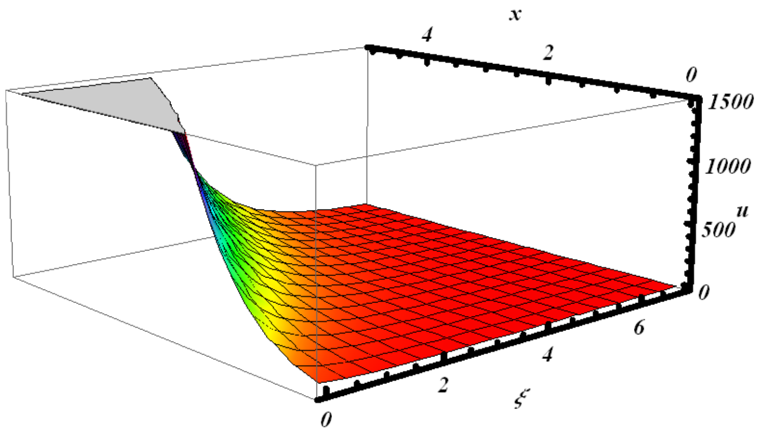

Fig. 10(b). 3D plot of u with ξ and x for
$Pr = 0.72, \varepsilon = 0.2, \theta_r = -5, \alpha = 0.5, m = 5, Mn = 1.5, \gamma = 5, \lambda = \beta = 0.2.$

Finally, Residual error graphs have been plotted in Figure 12 (a-c) for $f'(\xi)$ and $\theta(\xi)$ with different values of γ and λ. This clearly demonstrates the accuracy and convergence of OHAM. These figures show that a tenth-order approximation yields the best accuracy for the present model. The influence of various physical parameters on skin friction and Nusselt number are recorded in Table 4(a) and 4(b). Both skin friction $f''(0)$ and Nusselt number $\theta'(0)$ escalate for growing values of γ, ε and α, whereas the opposite trend is observed for $\Pr$ and m. With decreasing values of θ_r, β and Mn, $f''(0)$ increases and $\theta'(0)$ decreases.

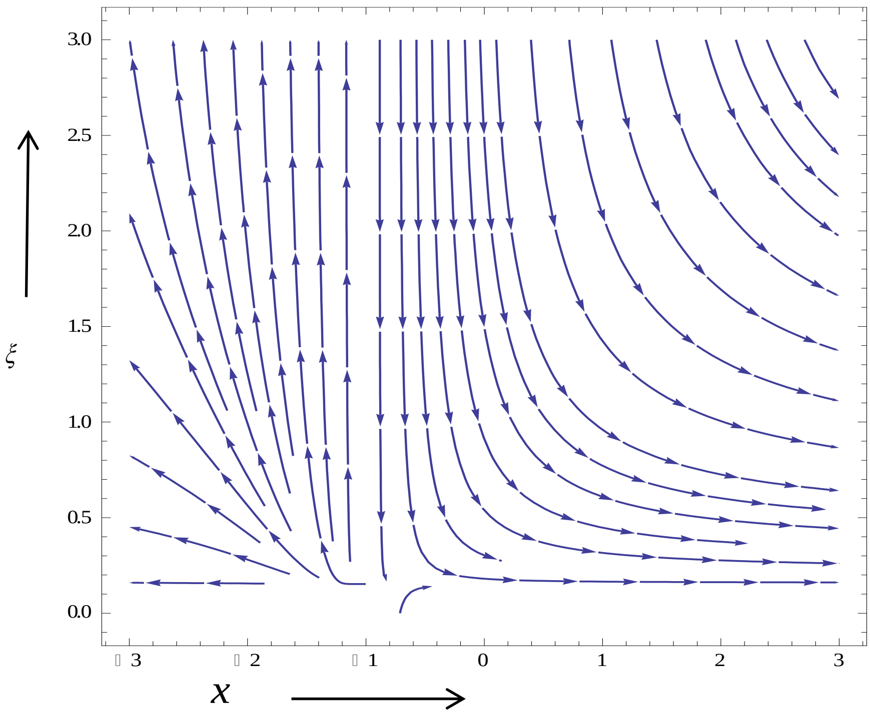

Fig. 11(a). Streamline pattern for
$\Pr = 0.72, \varepsilon = 0.1, \theta r = -5, \alpha = 0.2, Mn = 0.1, \gamma = 5, \lambda = 0.1, \beta = 0.1$

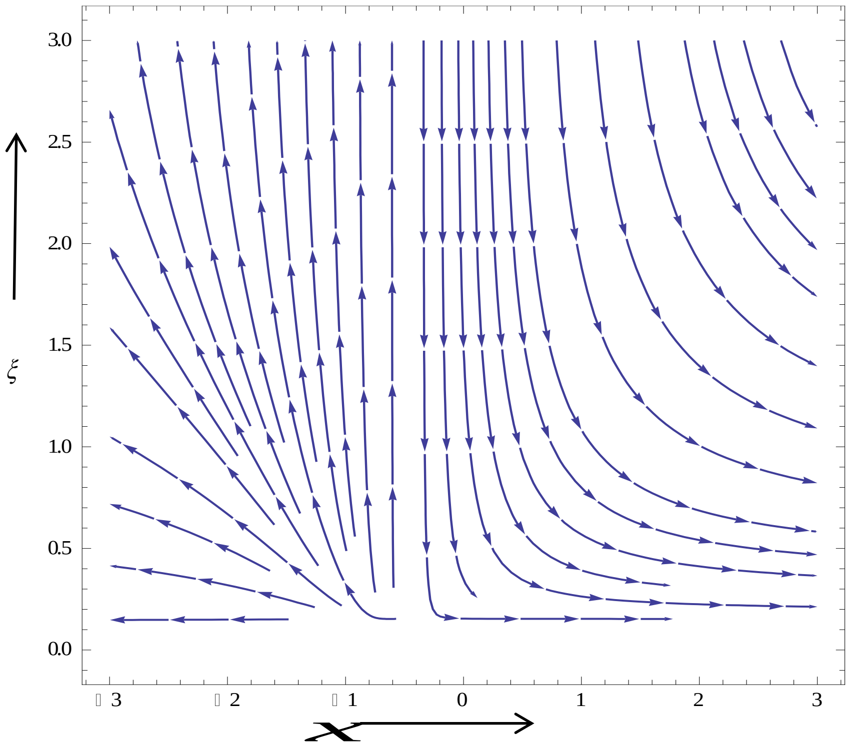

Fig. 11(b). Streamline pattern for
$\Pr = 0.72, \varepsilon = 0.1, \theta r = -5, \alpha = 0.2, Mn = 0.1, \gamma = 5, \lambda = 0.1, \beta = 0.1$

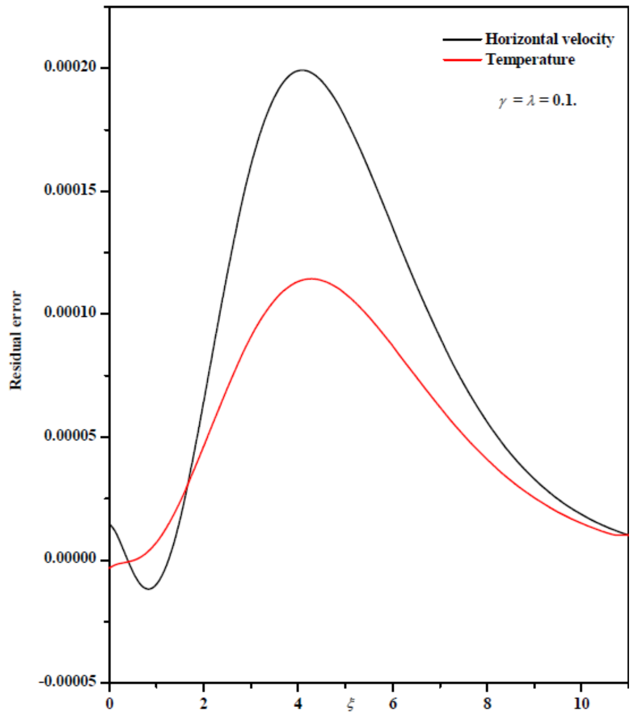

Fig. 12(a). Residual error profile for horizontal velocity and temperature with $\Pr = 0.72$, $\varepsilon = 0.1$, $\theta_r = -1$, $\alpha = 0.5$, $Mn = 0.1$, $m = 10$, $\beta = 0.1$

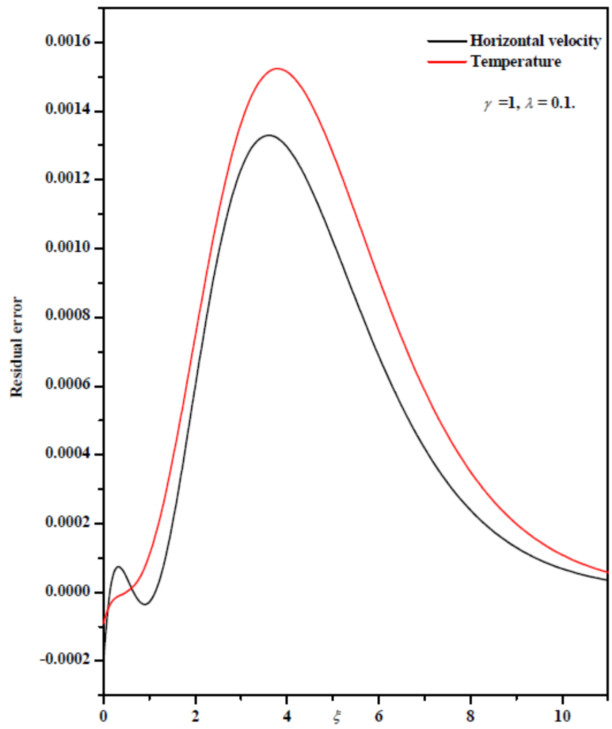

Fig. 12(b). Residual error profile for horizontal velocity and temperature with $\Pr = 0.72$, $\varepsilon = 0.1$, $\theta_r = -1$, $\alpha = 0.5$, $Mn = 0.1$, $m = 10$, $\beta = 0.1$

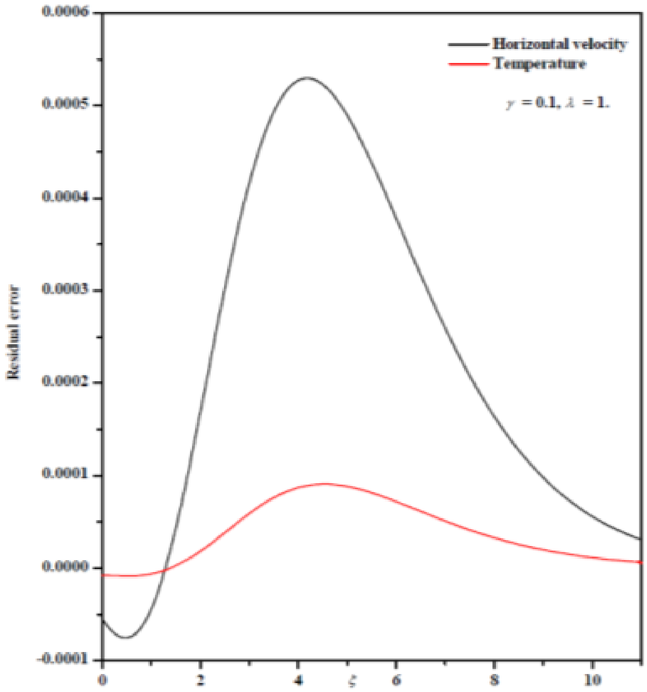

Fig. 12(c). Residual error profile for horizontal velocity and temperature with $\Pr = 0.72, \varepsilon = 0.1$, $\theta_r = -1$, $\alpha = 0.5$, $Mn = 0.1$, $m = 10$, $\beta = 0.1$

Table 1
Individual average residual error with $\Pr = 0.72,\ \varepsilon = 0.2,\ \theta_r \to -5,\ \alpha = 0.5,$ $m = 5,\ Mn = 1, \gamma = 5, \lambda = 0.2, \beta = 0.2.$

k	E_k^f	E_k^θ	CPU time (secs)
1	2.2×10^{-2}	2.1×10^{-2}	0.42
3	3.3×10^{-4}	1.5×10^{-3}	16.16
5	1.7×10^{-5}	1.7×10^{-4}	93.35
7	2.5×10^{-6}	1.2×10^{-5}	111.23
9	3.5×10^{-8}	2.5×10^{-7}	354.23
11	8.3×10^{-9}	1.5×10^{-7}	562.27
13	4.5×10^{-9}	7.8×10^{-8}	865.25
15	6.5×10^{-10}	3.5×10^{-8}	1232.30
17	1.8×10^{-10}	1.4×10^{-8}	1563.36
19	3.1×10^{-11}	8.2×10^{-9}	1986.54

Table 2
Values of convergence control parameters h_f and h_θ and the corresponding average residual errors E_k^f, E_k^θ *and* E_k^φ for a different order of approximation k with

k	h_f	E_k^f	h_θ	E_k^θ	CPU time (Secs)
1	-0.785657	3.0×10^{-3}	-0.199915	6.6×10^{-3}	3.19
3	-0.828322	7.4×10^{-5}	-1.002630	1.3×10^{-3}	25.48
5	-0.832214	5.7×10^{-6}	-1.042640	1.6×10^{-4}	110.42
7	-0.889803	2.2×10^{-6}	-1.056640	2.6×10^{-5}	351.42
9	-0.955139	8.7×10^{-7}	-1.065420	5.1×10^{-6}	970.99

Table 3
Comparison of results for $-f''(0)$ when $\text{Mn}=\varepsilon=\gamma=\beta=\lambda=0$ and $\theta_r \to \infty$

α	m	Fang *et al.,* [27] By Shoo. Meth.	Khader and Megahed [28] when $\lambda=0$ By Che. Spe. Meth.	Prasad *et al.,* [33]	Present work with OHAM				Relative error with		
					$-f''(0)$	$-\hbar_f$	$E_{10}{}^{f}$	CPU Time	Fang *et al.,* [27]	Khader and Megahed [28]	Prasad *et al.,* [33]
0.5	10	1.0603	1.0603	1.0605077120653874	1.0604	1.5425	1.2546×10^{-8}	245.22	0.00943	0.00943	0.00943
	9	1.0589	1.0588	1.0511040757424492	1.0511	1.8652	5.7854×10^{-8}	258.32	0.74207	0.73256	0.00000
	7	1.0550	1.0551	1.0552402381500168	1.0552	1.4875	8.8956×10^{-9}	452.2	0.01900	0.00947	0.00000
	5	1.0486	1.0486	1.048791366557854	1.0486	1.0253	4.2563×10^{-7}	452.32	0.00000	0.00000	0.00953
	3	1.0359	1.0358	1.035877993886442	1.0357	0.2547	2.3652×10^{-5}	236.14	0.01931	0.00965	0.00965
	2	1.0234	1.0234	1.0230051676018523	1.0230	1.8965	6.4512×10^{-6}	152.65	0.03910	0.03910	0.00000
	1	1.0000	1.0000	1.0	1.0000	1.0356	7.4587×10^{-9}	356.32	0.00000	0.00000	0.00000
	0.5	0.9799	0.9798	0.9791336007879321	0.9792	1.1201	5.2587×10^{-7}	258.26	0.07148	0.06127	0.01021
	0	0.9576	0.9577	0.9571649276940054	0.9571	1.6589	2.2356×10^{-5}	230.39	0.05224	0.06268	0.00000
	-1/3	1.0000	1.0000	0.999835549839111	1.0000	1.6125	1.9852×10^{-6}	298.72	0.00000	0.00000	0.02000
	-1/2	1.1667	1.1666	1.1668932098461453	1.1668	1.2912	1.3971×10^{-8}	329.16	0.00857	0.01714	0.00000
0.25	10	1.1433	1.1433	1.1439820336033696	1.1428	1.3520	8.7895×10^{-8}	324.58	0.04375	0.04375	0.09625
	9	1.1404	1.1404	1.1402440847765778	1.1403	0.2536	5.7562×10^{-9}	135.87	0.00876	0.00876	0.00876
	7	1.1323	1.1323	1.1329048196291788	1.1330	1.2578	2.9542×10^{-9}	324.68	0.06178	0.06178	0.00882
	5	1.1186	1.1186	1.1181398433389969	1.1181	1.6974	2.1364×10^{-7}	305.24	0.04471	0.04471	0.00000
	3	1.0905	1.0904	1.090832184327589	1.0908	0.9547	4.6425×10^{-7}	362.47	0.02750	0.03667	0.00000
	1	1.0000	1.0000	1.0	1.0000	0.4852	1.8541×10^{-7}	124.25	0.00000	0.00000	0.00000
	0.5	0.9338	0.9337	0.9330216794465643	0.9335	1.5412	7.9828×10^{-5}	278.56	0.03213	0.02142	0.05356
	0	0.7843	0.7843	0.7840615830209784	0.7842	1.2391	7.9965×10^{-8}	158.23	0.01275	0.01275	0.02550
	-1/3	0.5000	0.5000	0.49999454048648743	0.4999	1.2546	5.4458×10^{-8}	147.36	0.02000	0.02000	0.00000
	½	0.0833	0.08322	0.08330568175024846	0.0833	0.7984	2.2233×10^{-8}	267.35	0.00000	0.09603	0.00000

Table 4(a)
Values of Skin friction, the Nusselt number for $\alpha = 0.25$ and $\alpha = 0.5$ with different values of the physical parameters at 10th approximation

λ	ε	m	Pr	β	γ	Mn	θ_r	$\alpha = 0.25$		E_{10}^{t}	CPU time	$\alpha = 0.5$		E_{10}^{t}	CPU time
								$f''(0)$	$\theta'(0)$			$f''(0)$	$\theta'(0)$		
0.2	0.2	0.25	0.72	0.2	5.0	1.0	-10.0	-0.975517	-0.263838	1.235×10^{-7}	253.32	-1.030980	-0.314696	1.258×10^{-8}	214.25
							-7.0	-0.991000	-0.263627	7.815×10^{-8}	789.25	-1.047920	-0.305319	1.235×10^{-8}	365.25
							-5.0	-1.011010	-0.262361	3.542×10^{-8}	546.23	-1.069850	-0.216336	1.254×10^{-8}	785.36
							-2.0	-1.105690	-0.252399	1.445×10^{-8}	258.36	-1.173960	-0.200433	1.236×10^{-8}	415.25
		5.0				0.0	-5.0	-0.843308	-0.854416	5.235×10^{-8}	147.23	-0.795405	-0.833484	4.253×10^{-8}	523.3
						0.5		-0.981190	-0.812557	2.356×10^{-9}	458.36	-0.933456	-0.791419	4.356×10^{-8}	254.3
						1.0		-1.097060	-0.778025	1.235×10^{-7}	854.36	-1.049910	-0.756444	4.587×10^{-8}	335.2
						1.5		-1.196840	-0.749283	8.325×10^{-8}	965.23	-1.150570	-0.727252	6.325×10^{-8}	125.25
0.1	0.1	0.25		0.1	0.5	0.1		-0.836793	-0.380116	6.325×10^{-5}	874.52	-0.914069	-0.305458	5.326×10^{-8}	445.23
					1.0			-0.835475	-0.285370	4.256×10^{-8}	951.23	-0.916775	-0.285019	8.256×10^{-8}	855.33
					10.0			-0.833802	-0.261358	3.568×10^{-4}	753.25	-0.918271	-0.254592	9.256×10^{-8}	254.36
					50.0			-0.833821	-0.260022	7.235×10^{-8}	852.12	-0.918406	-0.213088	8.256×10^{-8}	452.36
					100			-0.833820	-0.257803	1.253×10^{-8}	365.25	-0.918423	-0.204144	2.365×10^{-8}	154.36
					500			-0.833819	-0.256448	6.325×10^{-9}	458.36	-0.918437	-0.185072	2.658×10^{-8}	854.36
					1000			-0.833819	-0.255511	9.325×10^{-8}	987.25	-0.917731	-0.160456	1.478×10^{-8}	785.36
					5000			-0.833819	-0.248682	4.253×10^{-7}	564.25	-0.917731	-0.120082	3.258×10^{-8}	852.36
0.2	0.2	10.0		0.1	5.0	1.0		-1.290910	-0.859849	1.235×10^{-8}	213.25	-1.218520	-0.833937	3.698×10^{-8}	369.25
				0.2				-1.304900	-0.819540	5.236×10^{-2}	685.25	-1.448870	-0.794853	2.589×10^{-8}	457.36
				0.3				-2.168918	-0.787125	5.289×10^{-5}	652.36	-1.823684	-0.763249	1.236×10^{-8}	321.5
		5.0	0.72	0.2				-1.097060	-0.778025	7.256×10^{-8}	452.36	-1.049910	-0.756444	4.569×10^{-8}	125.36
			1.0					-1.101800	-0.776090	9.325×10^{-8}	985.36	-1.054310	-0.875238	7.896×10^{-8}	558.36
			5.09					-1.125090	-1.761740	4.253×10^{-8}	214.36	-1.076260	-1.631510	9.998×10^{-8}	986.25
			6.2					-1.125830	-1.758900	9.253×10^{-8}	542.36	-1.077590	-1.729880	8.558×10^{-8}	456.35
		-0.2	0.72					-0.898399	0.516864	5.236×10^{-5}	954.33	-1.106300	0.141974	6.225×10^{-8}	325.36
		-0.1						-0.942342	0.200185	4.256×10^{-6}	225.36	-1.092130	-0.011930	4.285×10^{-8}	125.36
		0.0						-0.970429	0.005143	3.789×10^{-8}	558.36	-1.082810	-0.127024	3.693×10^{-8}	225.36
		1.0						-1.057520	-0.552852	5.874×10^{-8}	985.36	-1.057520	-0.552852	7.589×10^{-8}	365.25
		5.0						-1.097060	-0.778025	6.325×10^{-8}	125.36	-1.049910	-0.756444	3.564×10^{-8}	112.33
		10.0						-1.104900	-0.819540	8.325×10^{-8}	365.32	-1.048870	-0.794853	2.785×10^{-8}	125.36

Table 4 (b)
Values of Skin friction, the Nusselt number for $m=5$ and $m=10$ with different values of the physical parameters at 10th approximation

θ_r	ε	γ	λ	Pr	α	β	Mn	$m=5.0$ $f''(0)$	$m=5.0$ $\theta'(0)$	E_{10}^{t}	CPU time	$m=10.0$ $f''(0)$	$m=10.0$ $\theta'(0)$	E_{10}^{t}	CPU time
-5.0	0.2	5.0	0.2	0.72	0.5	0.2	0.0	-0.795405	-0.833484	2.565×10^{-8}	254.23	-0.804224	-0.872575	6.222×10^{-8}	852.32
							0.5	-0.933456	-0.791419	1.452×10^{-8}	558.25	-0.936344	-0.830488	2.002×10^{-8}	142.35
							1.0	-1.049910	-0.756444	3.256×10^{-8}	663.25	-1.048870	-0.794853	4.065×10^{-8}	356.25
							1.5	-1.150570	-0.727252	7.258×10^{-8}	889.25	-1.146850	-0.764626	8.223×10^{-8}	854.25
					0.25	0.1	1.0	-1.269460	-0.815560	9.665×10^{-8}	778.25	-1.290910	-0.859849	5.457×10^{-8}	654.32
						0.2		-1.297060	-0.778025	5.556×10^{-8}	563.25	-1.404900	-0.819540	2.568×10^{-8}	458.25
						0.3		-1.363224	-0.748001	9.547×10^{-8}	478.25	-2.968918	-0.787125	3.245×10^{-8}	987.45
					0.0	0.2		-1.143170	-0.799674	3.254×10^{-8}	658.25	-1.161670	-0.828367	9.254×10^{-8}	258.14
					0.2			-1.107380	-0.786852	1.475×10^{-8}	956.23	-1.116470	-0.824661	9.546×10^{-8}	102.30
					0.3			-1.088140	-0.777907	3.698×10^{-8}	854.78	-1.093440	-0.814455	4.235×10^{-8}	105.22
					0.5			-1.049910	-0.756444	2.589×10^{-8}	698.25	-1.048870	-0.794853	6.235×10^{-8}	542.32
				0.72	0.5			-1.049910	-0.756444	3.546×10^{-8}	215.35	-1.048870	-0.794853	7.258×10^{-8}	854.25
				1.0				-1.054310	-0.875238	3.896×10^{-8}	425.36	-1.053140	-0.918003	6.325×10^{-8}	326.25
				2.0				-1.064480	-1.174620	6.548×10^{-8}	548.25	-1.062730	-1.221120	1.003×10^{-8}	257.24
				5.0				-1.076260	-1.631510	6.458×10^{-8}	365.24	-1.073260	-1.671960	1.114×10^{-8}	124.35
				6.2				-1.077590	-1.729880	2.587×10^{-8}	124.35	-1.074420	-1.768220	3.445×10^{-8}	546.87
-2.0			-1.0	0.72	0.25			-1.623460	-0.620910	1.07×10^{-8}	653.24	-1.606310	-0.660658	5.558×10^{-8}	254.24
			0.0					-1.245370	-0.741499	2.365×10^{-8}	856.25	-1.248960	-0.781857	3.446×10^{-8}	125.25
			0.5					-1.092010	-0.788616	8.552×10^{-8}	456.23	-1.103870	-0.828829	3.889×10^{-8}	257.24
			1.0					-0.953553	-0.828163	9.665×10^{-8}	325.84	-0.972772	-0.868215	3.845×10^{-8}	256.34
			2.0					-0.709158	-0.890571	4.587×10^{-8}	658.25	-0.740951	-0.930120	4.589×10^{-8}	147.25

θ_r	ε	Pr	m	λ	α	β	Mn	$\gamma=5.0$		E_{10}^{t}	CPU time	$\gamma=10.0$		E_{10}^{t}	CPU time
-5.01	0.2	0.72	5.0	0.2	0.5	0.2	1.0	-1.049910	-0.756444	9.258×10^{-8}	740.25	-1.049930	-0.812900	8.235×10^{-8}	225.24
		1.0						-1.054310	-0.875238	6.254×10^{-8}	854.24	-1.054790	-0.951730	9.254×10^{-8}	114.25
		2.0						-1.064480	-1.174620	5.665×10^{-8}	125.25	-1.066660	-1.317480	3.245×10^{-8}	356.25
		5.09						-1.076260	-1.631510	3.224×10^{-8}	352.14	-1.082280	-1.925690	9.556×10^{-8}	986.25
		6.2						-1.077590	-1.729880	4.227×10^{-8}	114.25	-1.084660	-2.073710	8.457×10^{-8}	142.35
	0.1	0.72	0.25	0.5	0.5	0.1	0.1	-1.095180	-0.822558	2.325×10^{-7}	125.25	-0.959551	-0.862101	1.254×10^{-8}	546.32
	0.2							-1.092010	-0.788616	4.256×10^{-7}	753.25	-0.953553	-0.828163	1.587×10^{-7}	558.20
	0.3							-1.088990	-0.757956	1.025×10^{-9}	258.07	-0.947888	-0.797459	6.254×10^{-8}	856.32
	0.4							-1.086130	-0.730249	1.005×10^{-8}	825.25	-0.942535	-0.769565	4.221×10^{-8}	213.00

6. Conclusions

Few of the important findings are:

- Viscosity parameter reduces the momentum boundary layer thickness enhances the thermal boundary layer thickness.
- Biot number increases the temperature field for larger values which show that the convection is the principal heat transfer instrument.
- The role of wall thickness parameter α is to enhance both momentum and thermal boundary layer thickness.
- The dimensionless velocity at any point near the plate decrease as the wall thickness parameter increase for m < 1 and for and temperature distributions reduces for higher values of the wall thickness parameter when m < 1 and a reverse is true for m ≥ 1.
- Mixed convection parameter increases the velocity profile and intern enhances the momentum boundary layer thickness but lessens the thermal boundary layer thickness.

References

[1] Schneider, W. "A similarity solution for combined forced and free convection flow over a horizontal plate." *International Journal of Heat and Mass Transfer* 22, no. 10 (1979): 1401-1406.

[2] Dey, J. "Mixed convection flow over a semi-infinite horizontal plate with vectored mass transfer." *Journal of Heat Transfer* 104, no. 3 (1982): 558-560.

[3] Afzal, N. "Mixed convection over a horizontal plate." *J. Heat Transfer Trans. ASME* 106 (1984): 240-241.

[4] Ingham, D. B. "Singular and non-unique solutions of the boundary-layer equations for the flow due to free convection near a continuously moving vertical plate." *Zeitschrift für angewandte Mathematik und Physik ZAMP* 37, no. 4 (1986): 559-572.

[5] Wang, T-Y. "Mixed convection heat transfer from a vertical plate to non-Newtonian fluids." *International Journal of Heat and Fluid Flow* 16, no. 1 (1995): 56-61.

[6] Ali, M., and Fahd Al-Yousef. "Laminar mixed convection from a continuously moving vertical surface with suction or injection." *Heat and Mass Transfer* 33, no. 4 (1998): 301-306.

[7] Chen, C-H. "Laminar mixed convection adjacent to vertical, continuously stretching sheets." *Heat and Mass Transfer* 33, no. 5-6 (1998): 471-476.

[8] Chen, Chien-Hsin. "Magneto-hydrodynamic mixed convection of a power-law fluid past a stretching surface in the presence of thermal radiation and internal heat generation/absorption." *International Journal of Non-Linear Mechanics* 44, no. 6 (2009): 596-603.

[9] Subhashini, S. V., Nancy Samuel, and I. Pop. "Effects of buoyancy assisting and opposing flows on mixed convection boundary layer flow over a permeable vertical surface." *International Communications in Heat and Mass Transfer* 38, no. 4 (2011): 499-503.

[10] Makinde, O. D. "Heat and mass transfer by MHD mixed convection stagnation point flow toward a vertical plate embedded in a highly porous medium with radiation and internal heat generation." *Meccanica* 47, no. 5 (2012): 1173-1184.

[11] Srinivasacharya, D., and G. Swamy Reddy. "Chemical reaction and radiation effects on mixed convection heat and mass transfer over a vertical plate in power-law fluid saturated porous medium." *Journal of the Egyptian Mathematical Society* 24, no. 1 (2016): 108-115.

[12] Prasad, K. V., H. Vaidya, and K. Vajravelu. "MHD Mixed Convection Heat Transfer in a Vertical Channel with Temperature-Dependent Transport Properties." *Journal of Applied Fluid Mechanics* 8, no. 4 (2015).

[13] K. Vajravelu. K. V. Prasad, Hanumesh Vaidya, Neelufer Z. Basha, Chiu-On Ng. "Mixed Convective Flow of a Casson Fluid over a Vertical Stretching Sheet." *International Journal of Applied and Computational Mathematics*: 3(3) (2017) 1619-1638.

[14] Wakif, Abderrahim, Zoubair Boulahia, Mostafa Zaydan, Naoufal Yadil, and Rachid Sehaqui. "The power series method to solve a magneto-convection problem in a darcy-brinkman porous medium saturated by an electrically conducting nanofluid layer." *International Journal of Innovation and Applied Studies* 14, no. 4 (2016): 1048.

[15] Wakif, Abderrahim, Zoubair Boulahia, and Rachid Sehaqui. "Numerical study of the onset of convection in a newtonian nanofluid layer with spatially uniform and non uniform internal heating." *Journal of Nanofluids* 6, no. 1 (2017): 136-148.

[16] Wakif, Abderrahim, Zoubair Boulahia, and Rachid Sehaqui. "Numerical analysis of the onset of longitudinal convective rolls in a porous medium saturated by an electrically conducting nanofluid in the presence of an external magnetic field." *Results in physics* 7 (2017): 2134-2152.
[17] A. Wakif, Z.Boulahia F.A. Mohamed, R. Eid ,R. Sehaqui. "Numerical Analysis of the Unsteady Natural Convection MHD Couette Nanofluid Flow in the Presence of Thermal Radiation Using Single and Two-Phase Nanofluid Models for Cu–Water Nanofluids." *International Journal of Applied and Computational Mathematics* 4 (2018) 81.108.
[18] G. Manjunatha, C. Rajashekhari, "Slip effects on peristaltic transport of Casson fluid in an inclined elastic tube with porous walls." *Journal of Advanced Research in Fluid Mechanics and Thermal Sciences* : 43(1) (2018) 67-80.
[19] Choudhari, Rajashekhar, Manjunatha Gudekote, and Naveen Choudhari. "Analytical Solutions on the Flow of blood with the Effects of Hematocrit, Slip and TPMA in a porous tube." *Journal of Advanced Research in Fluid Mechanics and Thermal Sciences* 47, no. 1 (2018): 201-208.
[20] Aziz, Abdul. "A similarity solution for laminar thermal boundary layer over a flat plate with a convective surface boundary condition." *Communications in Nonlinear Science and Numerical Simulation* 14, no. 4 (2009): 1064-1068.
[21] Aziz, Abdul. "Hydrodynamic and thermal slip flow boundary layers over a flat plate with constant heat flux boundary condition." *Communications in Nonlinear Science and Numerical Simulation* 15, no. 3 (2010): 573-580.
[22] Makinde, Oluwole D., and A. Aziz. "Boundary layer flow of a nanofluid past a stretching sheet with a convective boundary condition." *International Journal of Thermal Sciences* 50, no. 7 (2011): 1326-1332.
[23] Bataller, Rafael Cortell. "Radiation effects for the Blasius and Sakiadis flows with a convective surface boundary condition." *Applied Mathematics and Computation* 206, no. 2 (2008): 832-840.
[24] Ishak, Anuar, Nor Azizah Yacob, and Norfifah Bachok. "Radiation effects on the thermal boundary layer flow over a moving plate with convective boundary condition." *Meccanica*46, no. 4 (2011): 795-801.
[25] Yao, Shanshan, Tiegang Fang, and Yongfang Zhong. "Heat transfer of a generalized stretching/shrinking wall problem with convective boundary conditions." *Communications in Nonlinear Science and Numerical Simulation* 16, no. 2 (2011): 752-760.
[26] Grosan, T., J. H. Merkin, and I. Pop. "Mixed convection boundary-layer flow on a horizontal flat surface with a convective boundary condition." *Meccanica* 48, no. 9 (2013): 2149-2158.
[27] Fang, Tiegang, Ji Zhang, and Yongfang Zhong. "Boundary layer flow over a stretching sheet with variable thickness." *Applied Mathematics and Computation* 218, no. 13 (2012): 7241-7252.
[28] Khader, M. M., and Ahmed M. Megahed. "Boundary layer flow due to a stretching sheet with a variable thickness and slip velocity." *Journal of Applied Mechanics and Technical Physics*56, no. 2 (2015): 241-247.
[29] Hayat, T., M. Farooq, A. Alsaedi, and Falleh Al-Solamy. "Impact of Cattaneo-Christov heat flux in the flow over a stretching sheet with variable thickness." *AIP Advances* 5, no. 8 (2015): 087159.
[30] Prasad, K. V., K. Vajravelu, and Hanumesh Vaidya. "Hall effect on MHD flow and heat transfer over a stretching sheet with variable thickness." *International Journal for Computational Methods in Engineering Science and Mechanics* 17, no. 4 (2016): 288-297.
[31] Prasad, K. V., H. Vaidya, K. Vajravelu, and M. M. Rashidi. "Effects of Variable Fluid Properties on MHD Flow and Heat Transfer over a Stretching Sheet with Variable Thickness." *Journal of Mechanics* 33, no. 4 (2017): 501-512.
[32] Prasad, K. V., K. Vajravelu, and Hanumesh Vaidya. "Hall effect on MHD flow and heat transfer over a stretching sheet with variable thickness." *International Journal for Computational Methods in Engineering Science and Mechanics* 17, no. 4 (2016): 288-297.
[33] Prasad, K. V., K. Vajravelu, Hanumesh Vaidya, and Robert A. Van Gorder. "MHD flow and heat transfer in a nanofluid over a slender elastic sheet with variable thickness." *Results in physics* 7 (2017): 1462-1474.
[34] Liao, Shi-Jun. "A new branch of solutions of boundary-layer flows over a permeable stretching plate." *International Journal of Non-Linear Mechanics* 42, no. 6 (2007): 819-830.
[35] Van Gorder, Robert A. "Optimal homotopy analysis and control of error for implicitly defined fully nonlinear differential equations." *Numerical Algorithms* (2018): 1-16.
[36] Prasad, K. V., K. Vajravelu, Hanumesh Vaidya, and S. R. Santhi. "Axisymmetric Flow of a Nanofluid Past a Vertical Slender Cylinder in the Presence of a Transverse Magnetic Field." *Journal of Nanofluids* 5, no. 1 (2016): 101-109.
[37] Prasad, K. V., K. Vajravelu, Hanumesh Vaidya, and B. T. Raju. "Heat transfer in a non-Newtonian nanofluid film over a stretching surface." *Journal of Nanofluids* 4, no. 4 (2015): 536-547.